THE JOURNAL OF BIOLOGICAL CHEMISTRY VOL. 286, NO. 18, pp. 15797–15805, May 6, 2011

Mouse Knock-out of IOP1 Protein Reveals Its Essential Role in Mammalian Cytosolic Iron-Sulfur Protein Biogenesis*◆

Received for publication, November 8, 2010, and in revised form, February 24, 2011 Published, JBC Papers in Press, March 2, 2011, DOI 10.1074/jbc.M110.201731

Daisheng Song and Frank S. Lee[1]

From the Department of Pathology and Laboratory Medicine, University of Pennsylvania School of Medicine, Philadelphia, Pennsylvania 19104

Iron-sulfur proteins play an essential role in a variety of biologic processes and exist in multiple cellular compartments. The biogenesis of these proteins has been the subject of extensive investigation, and particular focus has been placed on the pathways that assemble iron-sulfur clusters in the different cellular compartments. Iron-only hydrogenase-like protein 1 (IOP1; also known as nuclear prelamin A recognition factor like protein, or NARFL) is a human protein that is homologous to Nar1, a protein in *Saccharomyces cerevisiae* that, in turn, is an essential component of the cytosolic iron-sulfur protein assembly pathway in yeast. Previous siRNA-induced knockdown studies using mammalian cells point to a similar role for IOP1 in mammals. In the present studies, we pursued this further by knocking out *Iop1* in *Mus musculus*. We find that *Iop1* knock-out results in embryonic lethality before embryonic day 10.5. Acute, inducible global knock-out of *Iop1* in adult mice results in lethality and significantly diminished activity of cytosolic aconitase, an iron-sulfur protein, in liver extracts. Inducible knock-out of *Iop1* in mouse embryonic fibroblasts results in diminished activity of cytosolic but not mitochondrial aconitase and loss of cell viability. Therefore, just as with knock-out of *Nar1* in yeast, we find that knock-out of *Iop1/Narfl* in mice results in lethality and defective cytosolic iron-sulfur cluster assembly. The findings demonstrate an essential role for IOP1 in this pathway.

Iron-sulfur cluster proteins are an important class of proteins that contain iron-sulfur clusters in a variety of configurations, including [2Fe-2S] and [4Fe-4S] (1, 2). The distinctive redox and biophysical properties of these clusters make them suitable for a range of functions. Consequently, iron-sulfur proteins have diverse roles and participate in a broad range of biologic processes, including Krebs cycle reactions, oxidative phosphorylation, translation, iron regulatory pathways, and purine metabolism. Notably, these proteins exist in many cellular locales, including the cytosol, mitochondria, and nucleus.

How iron-sulfur cluster proteins are assembled in different cellular compartments has been an area of active investigation (3, 4). Iron-sulfur cluster assembly for all compartments originates in the mitochondria, and the initial step is catalyzed by a cysteine desulfurase that removes elemental sulfur from cysteine. The incorporation of this sulfur into iron-sulfur clusters then occurs by mechanisms that depend, in part, on cell compartment-specific machineries. Such a pathway exists, for example, for cytosolic iron-sulfur proteins. Important insights into this pathway, the cytosolic iron-sulfur protein assembly (CIA)[2] pathway, have been obtained from studies in *Saccharomyces cerevisiae* (3, 5). These studies have revealed a series of proteins that, in a stepwise fashion, assemble and deliver iron-sulfur clusters to target proteins. A current model is that the proteins Tah18 and Dre2 provide reducing equivalents for the assembly of iron-sulfur clusters on a scaffold that contains Cfd1 and Nbp35 (6–10). These clusters are then delivered to Nar1, which in conjunction with Cia1 then facilitates the insertion of the iron-sulfur clusters into appropriate apoproteins (11, 12). It should also be recognized that there is a role for other proteins, including proteins that have the following characteristics: they participate in iron-sulfur cluster biogenesis in the mitochondria, are predominantly mitochondrial in localization, but are also present at low levels in the cytosol (4, 13–17).

There is emerging evidence that this pathway is conserved in mammals (2, 3). Homologues for all of the aforementioned proteins have been identified in mammals, including humans. Functional data have been presented as well. We have employed siRNA to knockdown a human homologue of Nar1, IOP1/NARFL (18). These studies provided evidence for an important role for IOP1 in mammalian cytosolic iron-sulfur protein assembly. Other studies knocking down NBP35 in human cells in culture resulted in impaired cytosolic iron-sulfur cluster assembly (19). In both studies, mitochondrial iron-sulfur cluster assembly was unaffected. Functional studies implicating these human proteins have also been performed in yeast. Thus, human homologues of Dre2 (Ciapin1), Tah18 (Ndor1), and Cia1 (Ciao1) can functionally replace their yeast counterparts (8, 20).

It is notable in this regard that human IOP1 cannot functionally substitute for Nar1 in yeast (12). Moreover, humans possess an additional protein that is homologous to Nar1, which is called nuclear prelamin A recognition factor (NARF) and is distinct from IOP1/NARFL (21, 22). NARF was originally identified as a prelamin A-binding protein. These considerations

* This work was supported, in whole or in part, by National Institutes of Health Grant R01-GM71459 (to F. S. L.).

◆ This article was selected as a Paper of the Week.

[1] To whom correspondence should be addressed: Dept. of Pathology and Laboratory Medicine, University of Pennsylvania School of Medicine, 605 Stellar-Chance Labs, 422 Curie Blvd., Philadelphia, PA 19104. Tel.: 215-898-4701; Fax: 215-573-2272; E-mail: franklee@mail.med.upenn.edu.

[2] The abbreviations used are: CIA, cytosolic iron-sulfur protein assembly; IOP1, iron-only hydrogenase-like protein 1; IRP, iron regulatory protein; IRE, iron response element; MEF, mouse embryonic fibroblast; MTT, 3-(4,5-dimethylthiazol-2-yl)-2,5-diphenyltetrazolium bromide; NARF, nuclear prelamin A recognition factor; NARFL, nuclear prelamin A recognition factor-like protein; FRT, FLP recognition target; FLP, Flippase recombinase.

leave open the possibility that IOP1/NARFL (hereafter referred to as IOP1) might be redundant in function or perhaps not even relevant to the mammalian cytosolic iron-sulfur assembly pathway.

In these studies, we have genetically deleted *Iop1* in the mouse. We find that its deletion leads to lethality in the embryo, in the adult mouse, and in cells derived from these mice. We present evidence that *Iop1* deletion leads to a defect in cytosolic iron-sulfur protein assembly. Collectively, these findings lend strong support to a critical role for IOP1 in mammalian cytosolic iron-sulfur cluster assembly.

EXPERIMENTAL PROCEDURES

Gene Targeting—The construct targeting the mouse *Iop1* gene was prepared by recombineering (23). In brief, a minitargeting vector was constructed in the vector pL451 (24). This minitargeting vector contained genomic DNA encompassing exon 1 of the mouse *Iop1* gene with upstream and downstream loxP sites, a neomycin selection cassette flanked by FRT sites, and additional sequences downstream of exon 1. A retrieval plasmid was constructed in the vector pMC1-DTA (25). This retrieval plasmid contained sequences that flank 11.1 kb of genomic DNA sequence at the mouse *Iop1* locus, as well as a diphtheria toxin A negative selection cassette. This retrieval plasmid was used to capture, by recombineering, 11.1 kb of mouse *Iop1* genomic DNA containing exon 1 and exon 2 from C57BL/6 bacterial artificial chromosome clone RP23-377L13 (Invitrogen). The resulting product was then used, in the second recombineering step with the minitargeting vector, to generate the final targeting vector. This targeting vector contains an 8.0-kb 5′ arm, exon 1 with upstream and downstream loxP sites, a neomycin selection cassette flanked by FRT sites, and a 2.1-kb 3′ arm (see Fig. 1). Integrity of exons 1 and 2 was confirmed by DNA sequencing.

EAP6 C57BL/6 ES cells were electroporated with the targeting vector and selected using G418 at the University of Pennsylvania School of Medicine Gene Targeting Facility. Screening was performed by Southern blotting. One correctly targeted clone was identified, and it was injected into BALB/c blastocysts to generate chimeras at the University of Pennsylvania School of Medicine Transgenic Core Facility. Chimeric male mice were then mated with albino C57BL/6J-*Tyr*$^{c\text{-}2J}$ female mice (The Jackson Laboratory), and germline transmission was assessed by a combination of coat color and PCR. Mice with germline transmission of the targeted allele were then mated with C57BL/6-Tg(*ACTB-Flpe)2Arte* mice (Taconic) to delete the neomycin cassette followed by further crossing with C57BL/6 mice to segregate the *Flp* allele, thereby creating mice (*Iop1*$^{f/+}$) harboring an allele in which exon 1 has been flanked by loxP sites ("floxed") mice. *Iop1*$^{f/f}$ mice were obtained by crossing *Iop1*$^{f/+}$ mice.

Iop1$^{+/-}$ mice were generated by mating *Iop1*$^{f/f}$ mice with C57BL/6-Gt(*ROSA)26Sor*$^{tm16(Cre)Arte}$ mice (Taconic) followed by further crossing to segregate the *Cre* allele. *Iop1*$^{+/-}$ mice were crossed. In some crosses, timed matings were performed. *Iop1*$^{f/f}$; *Rosa26*-creER^{T2} mice were generated by crossing *Iop1*$^{f/f}$ mice with C57BL/6-Gt(*ROSA)26Sor*$^{tm9(cre/ESR1)Arte}$ mice (Taconic) followed by a second cross with *Iop1*$^{f/f}$ mice. *Iop1* knockout was induced in *Iop1*$^{f/f}$; *Rosa26*-creER^{T2} mice by administration of tamoxifen (MP Biomedicals) at a dose of 5 mg/day for up to 5 consecutive days by oral gavage.

All mice employed in this study were maintained in a C57BL/6 background. All animal procedures were approved by the Institutional Animal Care and Use Committees at the University of Pennsylvania in compliance with Animal Welfare Assurance.

Southern Blotting—Digoxigenin-labeled probes were generated by PCR using a PCR DIG probe synthesis kit (Roche Applied Science). For the 5′ probe (0.34 kb), the primers were 5′-CTC TCA CCA CAA GGA ATG-3′ and 5′-TTT TTA ATG GAG TCT ATC TGG-3′. For the 3′ probe (0.50 kb), the primers were 5′-AAG GCT CCG GAT ACA GAG-3′ and 5′-AAG AGT CTG GAA CCT CAG-3′. For both probes, bacterial artificial chromosome clone RP23-377L13 was employed as the template. Southern blotting was performed using DIG Easy Hyb, DIG wash and block buffer set, anti-digoxigenin-alkaline phosphatase conjugates, and CDP-Star substrate (all from Roche Applied Science).

PCR Genotyping—DNA was isolated from mouse tails (26). The following primers were employed for genotyping. For the 5′ loxP site (PCR product = 0.15 kb for wild type allele, 0.23 kb for floxed allele), the primers were: Iop LoxP5 primer = 5′-TTG AAA TGT AAA TAA AGA AAA TA-3′ and Iop LoxP3 primer = 5′-GCT GTT GAG ATG TTA AGA CTG GAG-3′. For the neomycin cassette (PCR product = 0.55 kb), the primers were: Iop Neo primer = 5′-CGC CTT CTT GAC GAG TTC TTC TG-3′ and Iop Com primer = 5′-GGC GGT CTG TCT GTA TCC CTC TC-3′. For the 3′ loxP site after neomycin cassette deletion (PCR product = 0.30 kb for wild type allele, 0.42 kb for floxed allele), the primers were: Iop Frt primer = 5′-CCT GGG ACC ATG GGA GTG TTT AG-3′ and Iop Com (see above). For the *Iop1* knock-out allele (PCR product = 0.75 kb), the primers were: Iop Del primer = 5′-CTA ATA GAC TTG GGT TTG GTG GTG-3′ and Iop Com (see above).

Mouse Embryonic Fibroblast (MEF) Generation—Murine fibroblasts were obtained from day 13.5 *Iop1*$^{f/f}$; *Rosa26*-creER^{T2} embryos by the primary explant technique (27) and then immortalized by transfection with pSG5-T, which contains the coding sequence for the SV40 large T antigen (28). MEFs were maintained in Dulbecco's modified Eagle's medium supplemented with 10% fetal bovine serum, 100 units/ml penicillin, and 100 μg/ml streptomycin. *Iop1* knock-out was induced with 250 nM 4-hydroxytamoxifen (Sigma) for 24 h.

Real Time PCR—RNA isolation and real time PCR were performed as described previously using a SYBR Green master mix (Applied Biosystems) (18). The following primers were employed to measure *Iop1* and ferritin heavy chain (*Fth*) messages in mouse RNA samples: *Iop1*, 5′-GGG CTC CCT GGT CAA AGA C-3′ and 5′-TGG TAG ATC TTG TCA GGA GTC AGA AG-3′; *Fth*, 5′-AAG ATG GGT GCC CCT GAA G-3′ and 5′-CCA GGG TGT GCT TGT CAA AGA-3′. Dissociation curve analysis revealed a single peak. The sequences of other real time PCR primers has been described (29). Relative quantification was performed employing the ΔΔCt method and β-actin as the endogenous control.

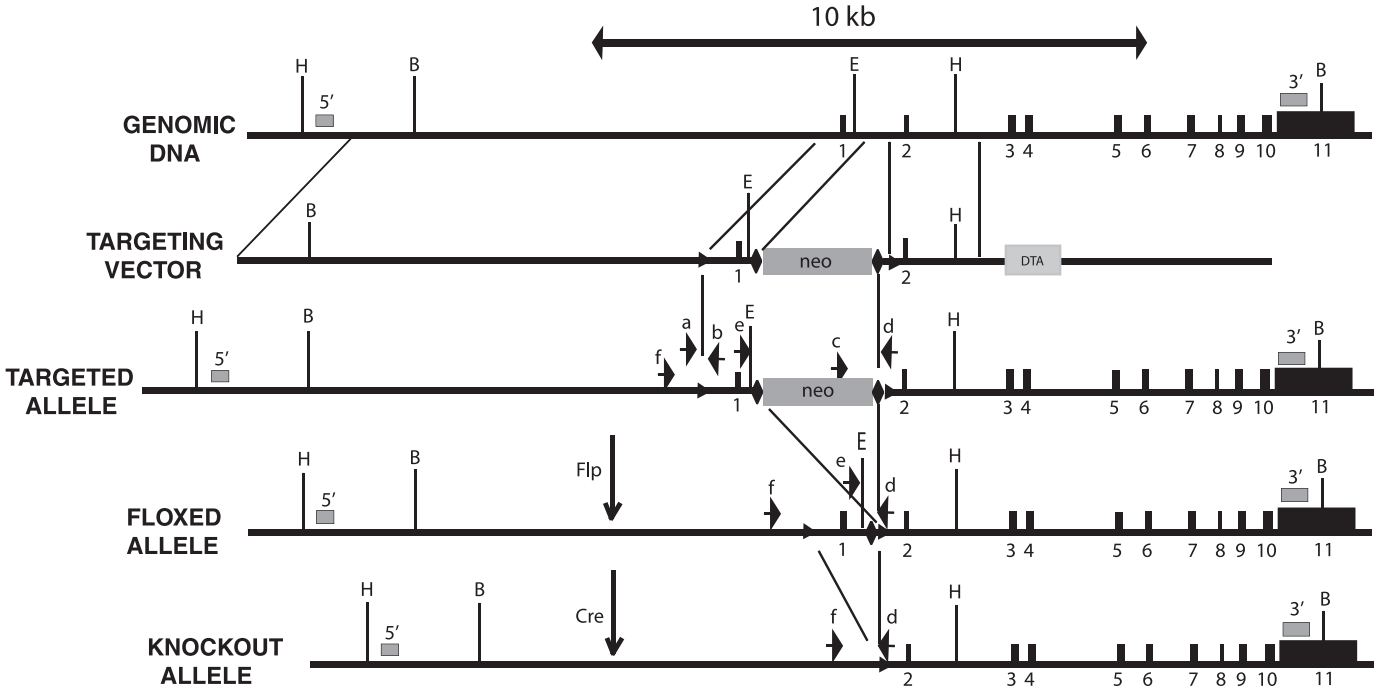

FIGURE 1. ***Iop1* gene targeting strategy.** *Black boxes* indicate exons. *Numbers* below boxes indicate exon number. Positions of 5′ and 3′ Southern probes are indicated by *gray boxes* and are denoted by 5′ and 3′, respectively. Positions of loxP and FRT sites are indicated by *triangles* and *diamonds*, respectively. Genotyping primers are denoted by *arrows* and are as follows: *a* = Iop LoxP5; *b* = Iop LoxP3; *c* = Iop Neo; *d* = Iop Com; *e* = Iop Frt; *f* = Iop Del. Restriction enzyme sites are as follows: *B* = BamHI; *E* = EcoRV; *H* = HpaI. *neo*, neomycin cassette; *DTA*, diphtheria toxin A-chain cassette.

Antibodies and Western Blotting—Antibodies to p38 (sc-728), JNK (sc-571), ERK (sc-93), and β-tubulin (sc-9104) were obtained from Santa Cruz Biotechnology. Antibodies against caspase 3 (catalogue number 9665), phospho-p38 (Thr-180/Tyr-182) (catalogue number 4631), phospho-JNK/SAPK (Thr-183/Tyr-185) (catalogue number 9251), and phospho-ERK1/2 (Thr-202/Tyr-204) (catalogue number 4370) were obtained from Cell Signaling Technologies. Antibodies against microtubule-associated light chain 3 (LC3; catalogue number AM1800) were obtained from Abgent. Antibodies against iron regulatory protein 2 (IRP2) were obtained from Novus Biologicals (NB100-1797). Antibodies to IOP1-(417–476) and cytochrome *c* have been described (18, 22). Western blotting was performed essentially as described (22). Typically, 30 μg of cell lysate were subjected to SDS-PAGE, and the proteins were transferred to polyvinylidene difluoride membranes. The membranes were blocked with 10% nonfat milk in phosphate-buffered saline containing 0.05% Tween 20 and probed with primary antibodies followed by horseradish peroxidase-coupled secondary antibodies. Detection was performed using SuperSignal substrate (Pierce).

Extract Preparation, Enzyme Assays, and EMSA—Liver extracts from *Iop1*$^{f/f}$ or *Iop1*$^{f/f}$*; Rosa26*-creER^{T2} mice were prepared as follows. Three days after the initial tamoxifen dose, mice were sacrificed by CO_2 inhalation. Livers were isolated, rinsed in PBS, and then minced and homogenized in ice-cold 100 mM Hepes, pH 7.4, 250 mM sucrose, 0.01% digitonin, and mammalian protease inhibitor mixture (Sigma). After 10 min on ice, the suspension was centrifuged at 300 × *g* for 5 min at 4 °C to remove tissue debris. The supernatant was then centrifuged at 10,000 × *g* for 10 min at 4 °C. The resulting supernatant was designated as the cytosolic fraction. The cell pellets were further washed three times in the same buffer employed for homogenization with a 1-min centrifugation at 3,000 × *g* after each wash. The pellet was then lysed in 100 mM Hepes, pH 7.4, 0.5% Triton X-100, and mammalian protease inhibitor mixture. After 10 min on ice, the lysate was centrifuged at 10,000 × *g* for 10 min at 4 °C. The supernatant from this centrifugation was designated as the mitochondrial fraction. For MEFs, cytosolic and mitochondrial extracts were prepared as described previously (16, 18). Protein concentrations of extracts were measured using a DC protein assay kit (Bio-Rad).

Aconitase, lactate dehydrogenase, citrate synthase, and xanthine oxidase activities were measured as described (16, 18). An MTT assay was performed using a kit from ATCC (catalogue number 30-1010K). EMSA was performed as described (18).

Fluorescence Microscopy—Cells were exposed to 500 nM MitoTracker Red CMXRos (Invitrogen) for 30 min. Images were obtained using an Olympus BX60 fluorescence microscope.

Statistical Analysis—Student's *t* test was used for statistical analysis. Significant differences were considered when $p < 0.05$. Data are presented as the mean ± S.D.

RESULTS

Mus musculus possesses orthologues of the two members of the human IOP family, which are IOP1/Narfl and IOP2/Narf, therefore making this species appropriate for the study of IOP1. To pursue this, our strategy was to knock out the *Iop1* gene in the mouse, as outlined in Fig. 1. The murine *Iop1* gene in chromosome 17 contains 11 exons. Exon 1 contains coding sequence for amino acids 1–22 of Iop1, which includes the initiator methionine codon. We chose to target this exon and associated upstream promoter sequences for deletion by flanking it

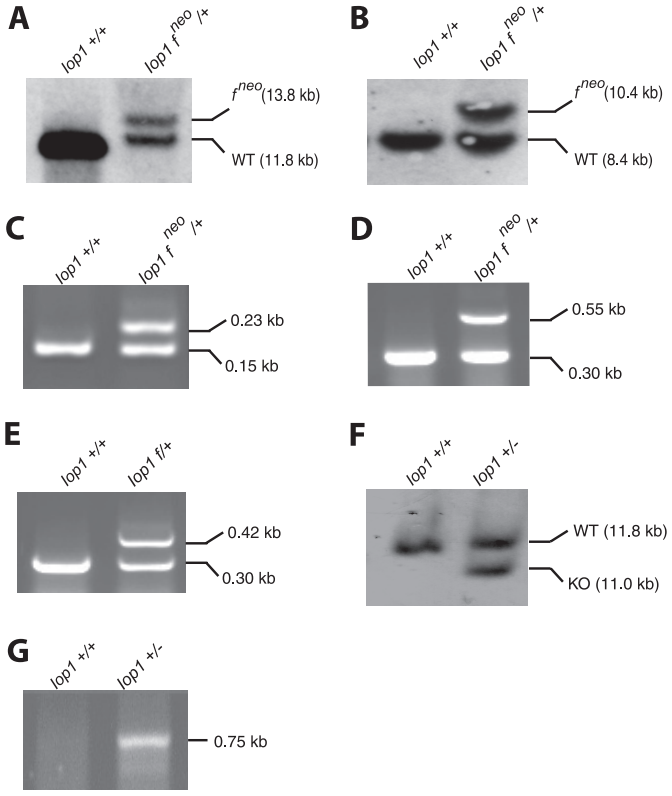

FIGURE 2. **Southern blotting and PCR confirmation of *Iop1* gene targeting.** *A* and *B*, Southern blots of ES cell DNA digested with HpaI (*A*) or BamHI/EcoRV (*B*) and hybridized with 5′ (*A*) or 3′ (*B*) Southern probes, respectively. The positions of the targeted allele (which contains the neomycin cassette) are indicated by f^{neo}. *C–E* and *G*, PCR was performed on tail DNA to assess the presence of the 5′ loxP site (Iop LoxP5 and Iop LoxP3 primers) (*C*) and the neomycin cassette (Iop Neo and Iop Com primers; Iop Frt primer was also included to allow detection of the wild type allele at 0.30 kb) (*D*), the 3′ loxP site following deletion of the neomycin cassette (Iop Frt and Iop Com primers) (*E*), and the *Iop1* knock-out allele (Iop Del and Iop Com primers) (*G*). The sizes of the PCR products are as indicated. *Iop1* genotypes of the DNA samples are indicated above the gels. *Iop1 f* denotes the presence of the floxed allele in the absence of the neomycin cassette. *F*, Southern blot of tail DNA digested with HpaI and hybridized with the 5′ Southern probe.

with loxP sites. It might be noted that upon deletion of exon 1, the next available exonic ATG is present in exon 2, and this ATG is out of frame with respect to the Iop1 coding sequence. We therefore conclude that this strategy should yield a null allele. The targeting vector contains 5′ and 3′ homology arms, as well as neomycin positive selection and diphtheria toxin negative selection cassettes.

C57BL/6 ES cells were electroporated with the targeting construct and then selected using G418. Of 300 clones screened by Southern blotting, one clone was identified with correct 5′ recombination and 3′ recombination events. Southern blotting with a 5′ probe reveals the expected 13.8-kb band upon hybridization with HpaI-digested DNA (Fig. 2*A*), whereas Southern blotting with a 3′ probe reveals the expected 10.4-kb band upon hybridization with BamHI/EcoRV-digested DNA (Fig. 2*B*).

This ES cell clone was injected into BALB/c blastocysts, resulting in eight male chimeras. The male chimeras were mated to C57BL/6 females, and two of the male chimeras yielded litters with germline transmission, as assessed by black coat color and PCR genotyping. PCR analysis of tail DNA revealed the integrity of the 5′ loxP site as well as the presence of

TABLE 1
Genotypes of embryos and pups produced from *Iop1*$^{+/-}$ intercrosses

Values are given as a percentage of total analyzed at a given stage. In parentheses, the data show the number observed with a given genotype/total number analyzed at a given stage. E10.5, embryonic day 10.5.

Genotype	% expected	Stage of development	
		E10.5 (4 litters)	Live birth (10 litters)
Iop1$^{+/+}$	25	44 (19/42)	64 (35/55)
Iop1$^{+/-}$	50	55 (23/42)	36 (20/55)
Iop1$^{-/-}$	25	0	0

the neomycin cassette (Fig. 2, *C* and *D*, respectively). The neomycin cassette, which is flanked by FRT sites, was removed by breeding correctly targeted mice with mice expressing Flp recombinase. Its removal was confirmed by PCR (Fig. 2*E*). We then obtained *Iop1*$^{f/f}$ mice, which were fertile and phenotypically normal, consistent with the absence of adverse effects from the loxP sites.

We generated *Iop1*$^{+/-}$ mice by breeding the *Iop1*$^{f/f}$ mice with mice expressing Cre recombinase. Southern blotting of HpaI-digested DNA with the 5′ probe reveals an 11.8-kb band corresponding to the wild type allele and an additional 11.0-kb band indicative of deletion of exon 1 and the associated upstream promoter (Fig. 2*F*). PCR analysis using primers that flank the original 5′ and 3′ loxP sites is also consistent with the expected deletion (Fig. 2*G*). These mice were fertile and without any gross abnormality.

We crossed *Iop1*$^{+/-}$ heterozygous mice to determine whether we could obtain *Iop1*$^{-/-}$ mice. Of 55 live births, none were *Iop1*$^{-/-}$ (Table 1). In addition, *Iop1*$^{+/-}$ mice were born in numbers lower than the expected Mendelian frequency, suggesting that *Iop1* haploinsufficiency has a deleterious effect during embryogenesis. We examined embryos at embryonic day 10.5 ($n = 42$) and likewise failed to observe any *Iop1*$^{-/-}$ embryos. Interestingly, the ratio of *Iop1*$^{+/-}$ heterozygotes to wild type mice at embryonic day 10.5 is higher than that observed at birth, further supporting a deleterious effect of *Iop1* haploinsufficiency during embryogenesis. From these studies, we conclude that knock-out of *Iop1* results in embryonic lethality in the mouse at a day earlier than embryonic day 10.5.

It is formally possible that *Iop1* serves a essential functional role only during embryogenesis but not later in life. To address this, as well as circumvent the embryonic lethality of *Iop1* knock-out, we generated a temporally inducible conditional knock-out of *Iop1*. We crossed the *Iop1*$^{f/f}$ mice with mice bearing a tamoxifen-inducible Cre recombinase (creER^{T2}). The latter mouse line expresses the modified Cre from the *Rosa26* locus, which allows a broad tissue expression (30). We then employed this *Iop1*$^{f/f}$; *Rosa26*-creER^{T2} mouse line to globally delete *Iop1* in the adult mouse. Toward this end, we treated adult mice with tamoxifen to induce *Iop1* deletion. We observed 100% lethality after 5 days following tamoxifen treatment ($n = 4$). *Iop1*$^{f/f}$ controls, in contrast, were completely viable and phenotypically normal following the same treatment ($n = 4$).

We examined mice at an earlier time point. We treated *Iop1*$^{f/f}$ and *Iop1*$^{f/f}$; *Rosa26*-creER^{T2} mice with tamoxifen. Three

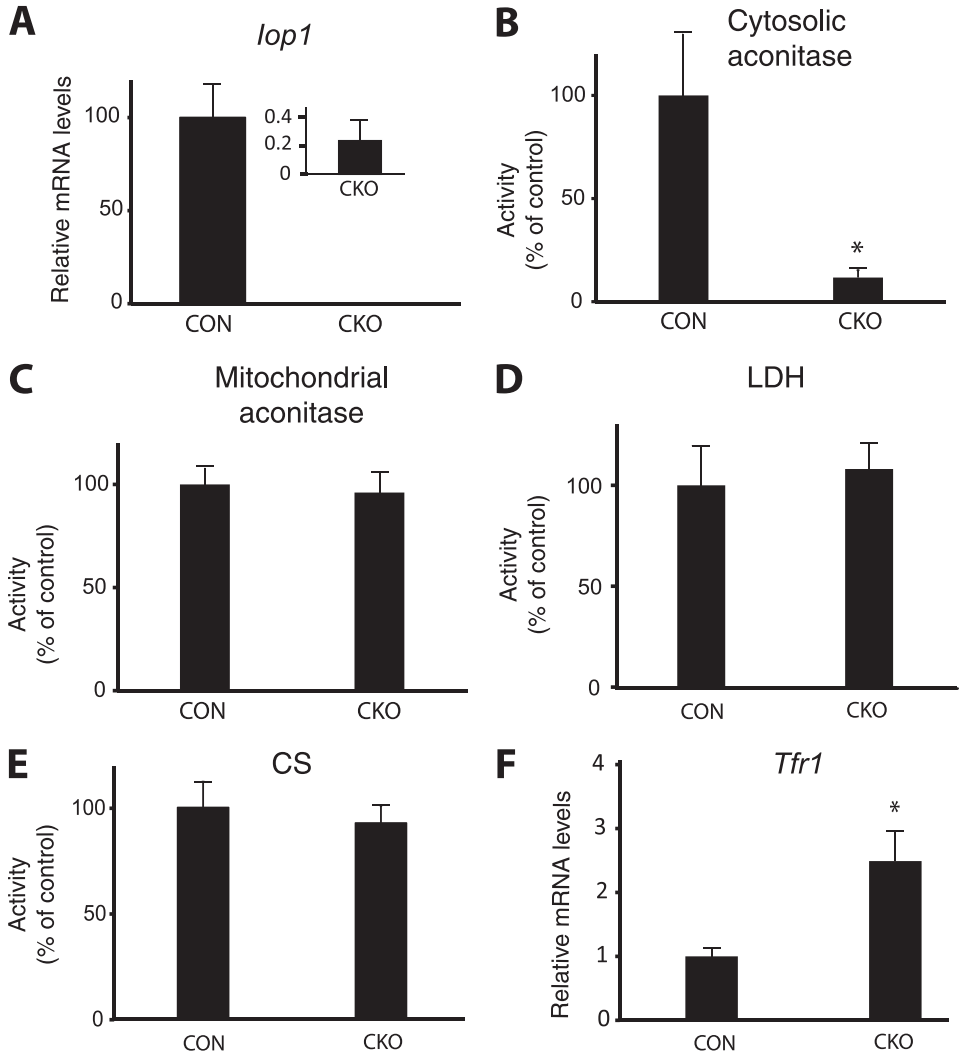

FIGURE 3. **Acute deletion of *Iop1* in adult mice.** Control (*CON*; *Iop1*$^{f/f}$) or conditional knock-out (*CKO*; *Iop1*$^{f/f}$; *Rosa26*-creER^{T2}) mice at 6–7 weeks of age were treated with tamoxifen for three consecutive days. After the last tamoxifen dose, livers were harvested, and both RNA and protein extracts were prepared. *A* and *F*, levels of *Iop1* (*A*) or *Tfr1* (*F*) message were quantitated by real time PCR ($n = 3$). *B–E*, activities of cytosolic aconitase (*B*), mitochondrial aconitase (*C*), lactate dehydrogenase (*LDH*) (*D*), or citrate synthase (*CS*) (*E*) were measured ($n = 3$). Data are presented as mean ± S.D. * indicates $p < 0.01$.

days after the initial tamoxifen dose, we isolated liver RNA and confirmed, by real time PCR, loss of the *Iop1* message (Fig. 3*A*). We prepared liver extracts and measured the activities of a number of enzymes. We find that *Iop1* knock-out results in substantial loss of activity of the iron-sulfur cluster protein cytosolic aconitase (Fig. 3*B*). Specificity for cytosolic iron-sulfur proteins is supported by the observation that mitochondrial aconitase activity is preserved (Fig. 3*C*). Further support for specificity is provided by the observation that the activities of two non iron-sulfur enzymes, lactate dehydrogenase (a cytosolic enzyme) and citrate synthase (a mitochondrial enzyme), are not significantly changed (Fig. 3, *D* and *E*).

Upon loss of its active site iron-sulfur cluster, cytosolic aconitase is converted to IRP1. IRP1 binds to iron response elements (IREs) in the mRNAs encoding proteins involved in iron homeostasis (31, 32). Multiple IREs reside in the 3′-untranslated region (UTR) of the transferrin receptor 1 (*Tfr1*) mRNA. Binding of IRP1 to this IRE serves to stabilize the *Tfr1* mRNA. Measurements of *Tfr1* message in the liver reveal an increase upon *Iop1* knock-out, consistent with conversion of cytosolic aconitase to Irp1 (Fig. 3*F*).

We isolated and then immortalized MEFs from *Iop1*$^{f/f}$; *Rosa26*-creER^{T2} embryos. When these cells were then treated with 4-hydroxytamoxifen, we observed a dramatic reduction in *Iop1* message (Fig. 4*A*). Examination of extracts by Western blotting using anti-IOP1 antibodies reveals a substantial loss of the protein after 1 day and almost no detectable Iop1 by 2 days (Fig. 4*B*). These results are consistent with the deletion producing a null allele.

We measured the viability of these MEFs following tamoxifen treatment. By either trypan blue exclusion or MTT assay, we observed reduced viability occurring as early as 3 days after tamoxifen treatment, with almost complete loss of viability at 5 days (Fig. 4, *C* and *D*). The decrease in viability was delayed with respect to loss of Iop1 protein. Examination of cells using the fluorescent dye MitoTracker Red CMXRos at 5 days after tamoxifen treatment confirmed substantial loss of viability, with only scattered cells maintaining mitochondrial integrity (compare Fig. 4*F* with Fig. 4*E*).

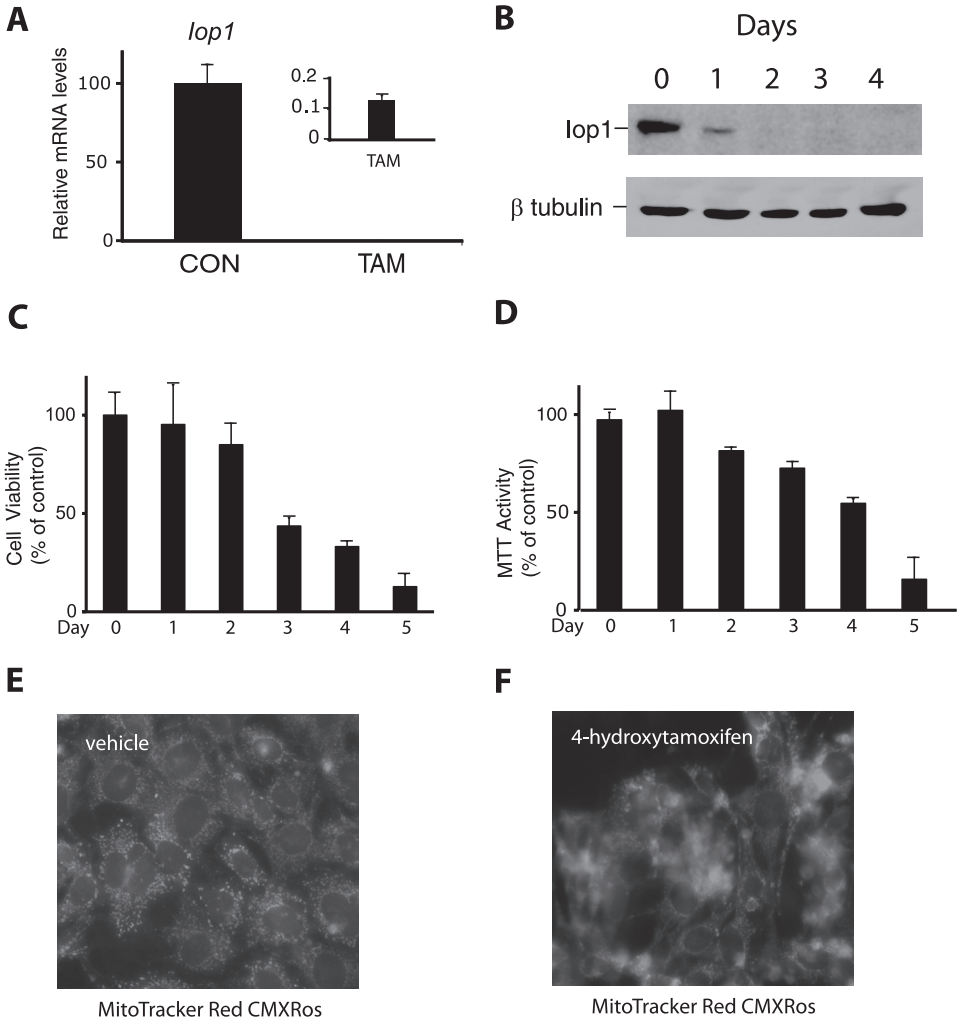

FIGURE 4. **Acute deletion of *Iop1* in MEFs.** *Iop1$^{f/f}$; Rosa26*-creER^{T2} MEFs were treated with either vehicle (ethanol as control (*CON*)) or 4-hydroxytamoxifen (*TAM*). *A*, RNA was isolated 48 h after treatment, and *Iop1* mRNA levels were assessed by real time PCR ($n = 3$). *B*, whole cell extracts were prepared from tamoxifen-treated *Iop1$^{f/f}$; Rosa26*-creER^{T2} MEFs at the indicated times and then examined by Western blotting using the indicated antibodies. *C* and *D*, cell viability was assessed by either trypan blue exclusion (*C*) or MTT assay (*D*) ($n = 3$ for each). Data are presented as mean ± S.D. *E* and *F*, *Iop1$^{f/f}$; Rosa26*-creER^{T2} MEFs were treated with vehicle (*E*) or 4-hydroxytamoxifen (*F*). Five days later, MitoTracker Red CMXRos (500 nM) was added for 30 min before examination by fluorescence microscopy. Images are at 400× magnification.

The delay between loss of Iop1 protein and loss of cell viability provided a window in which to pursue molecular studies. We harvested cells at 3 days after tamoxifen treatment, a time at which Iop1 protein expression has been lost, but importantly, before cell viability is almost completely comprised. We prepared cytosolic and mitochondrial fractions, which show the expected presence of tubulin and cytochrome *c*, respectively (Fig. 5*A*). We then measured enzyme activities. As shown in Fig. 5*B*, we find that Iop1 knock-out results in substantial loss of activity of cytosolic aconitase (38% of control, $p < 0.01$). We did not find any difference in activity in mitochondrial aconitase, nor did we observe changes in cytosolic lactate dehydrogenase or mitochondrial citrate synthase (Fig. 5, *C–E*). We examined xanthine oxidase, a cytosolic iron-sulfur cluster enzyme distinct from cytosolic aconitase, and find that its activity was also decreased (Fig. 5*F*).

Measurements of *Tfr1* mRNA reveal an increase upon Iop1 deletion, consistent with increased Irp1 activity due to loss of iron-sulfur cluster (Fig. 5*G*). In contrast, no significant change in ferritin heavy chain mRNA levels was seen following Iop1 deletion (Fig. 5*H*). Irp1 binds to an IRE in the 5′-UTR of the ferritin heavy chain mRNA, thereby serving to inhibit translation (31, 32). We find that *Iop1* knock-out leads to decreased ferritin heavy chain protein (Fig. 6*A*, *second panel* from *top*). We as well as others have observed that the apo form of IRP1 is less stable than the iron-replete form (18, 33, 34). Consistent with this, Irp1 protein levels also decline upon Iop1 knock-out (Fig. 6*A*, *third panel* from *top*) whereas Irp2 protein levels remain the same (Fig. 6*A*, *fourth panel* from *top*).

We performed electrophoretic mobility shift assays with cytoplasmic extracts prepared from these cells using a ^{32}P-labeled RNA probe containing the ferritin heavy chain IRE from the 5′-UTR. Consistent with previous observations employing extracts from murine cells (35–37), we observed two bands with this assay; the more slowly migrating band corresponds to Irp1-bound probe, and the more rapidly migrating one corresponds to Irp2-bound probe (Fig. 6*B*, *top panel*). After *Iop1* knock-out (for example, at 2 days following 4-hydroxytamoxifen treatment), we find an increase in the Irp1 gel shift (compare the *top band* in the *first two lanes* of the *top panel*) despite

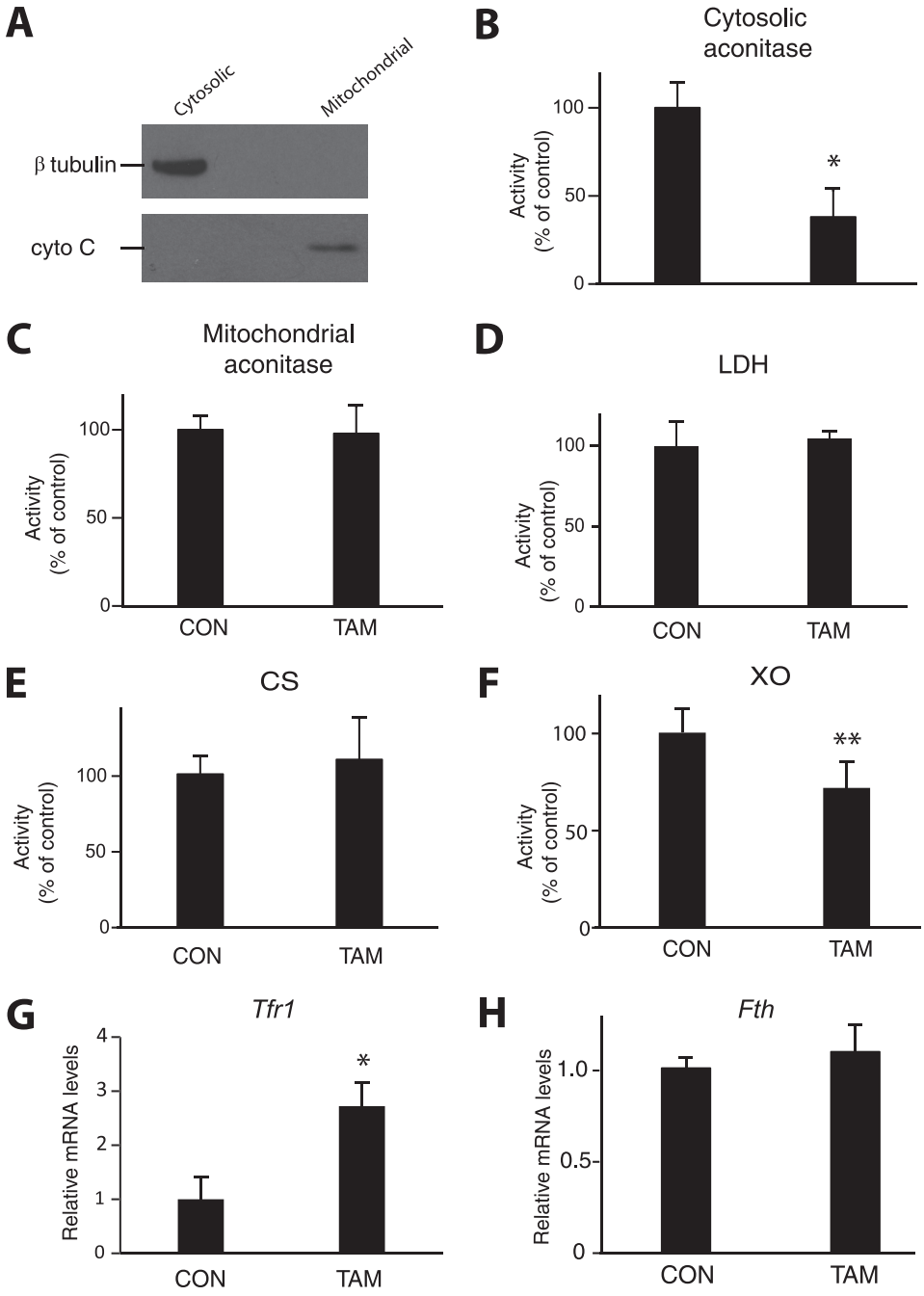

FIGURE 5. **Assay of enzymes and *Tfr1* message in extracts following *Iop1* deletion in MEFs.** *Iop1*$^{f/f}$; *Rosa26*-creER^{T2} MEFs were treated with either vehicle (ethanol as control (*CON*)) or 4-hydroxytamoxifen (*TAM*). *A*, 3 days later, cytosolic and mitochondrial extracts (10 μg) were analyzed by Western blotting using anti-β-tubulin or anti-cytochrome *c* antibodies. *B–F*, activities of cytosolic aconitase (*B*), mitochondrial aconitase (*C*), lactate dehydrogenase (*LDH*) (*D*), citrate synthase (*CS*) (*E*), and xanthine oxidase (*XO*) (*F*) were measured ($n = 3$). * indicates $p < 0.01$, and ** indicates $p < 0.05$. *G* and *H*, levels of *Tfr1* (*G*) and *Fth* (*H*) message were quantitated by real time PCR ($n = 3$). * indicates $p < 0.01$. Data are presented as mean ± S.D.

the observation that Irp1 protein levels decrease (Fig. 6*B*, *middle panel*). We also note a slight increase in the Irp2 gel shift (Fig. 6*B*, *top panel*), suggesting a minor contribution from this Irp isoform. Taken together, the data support the acquisition of functional Irp1 activity following *Iop1* knock-out.

To further explore loss of viability upon *Iop1* knock-out in MEFs, we examined a number of stress-induced pathways. We find that Iop1 loss results in induction of apoptosis, as evidenced by conversion of full-length caspase 3 to cleaved caspase 3 (Fig. 6*C*, *top panel*). Caspase 3 is a key effector caspase in apoptosis, and its activation occurs by cleavage (38). Interestingly, we also find evidence of induction of autophagy, as seen by the conversion of microtubule-associated light chain 3 I (LC3 I) to LC3 II (Fig. 6*C*, *second panel* from *top*). This conversion occurs during the formation of autophagosomes (39, 40). Protein kinases can also be induced by stress (41). Indeed, we find evidence of activation of p38, a major stress-induced kinase (Fig. 6*C*, *third panel* from *top*). Selectivity for this particular member of the MAPK family of protein kinases is provided by the observation that Jnk and Erk were not activated under the

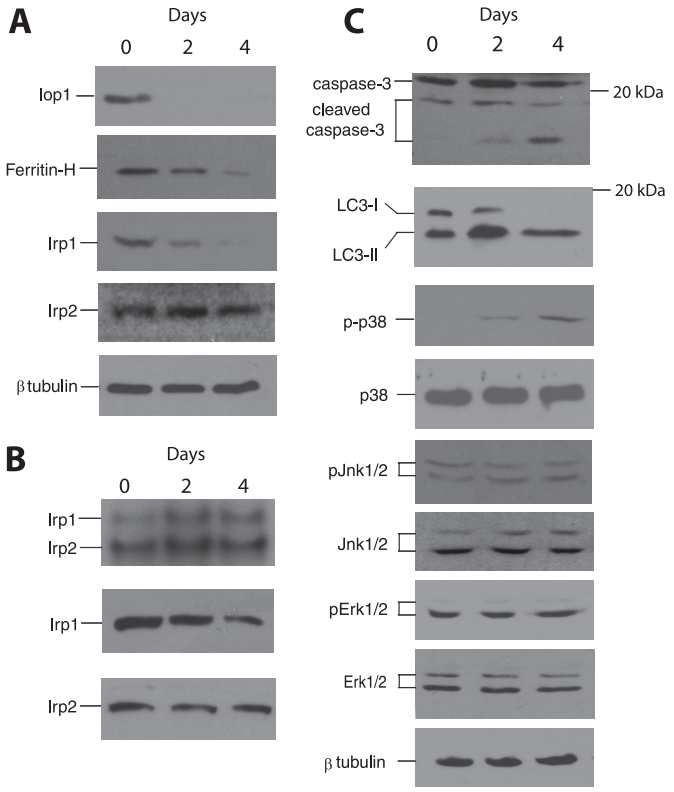

FIGURE 6. **Activation of selective intracellular pathways following *Iop1* deletion in MEFs.** *A*, *Iop1*$^{f/f}$; *Rosa26*-creER^{T2} MEFs were treated with 4-hydroxytamoxifen for the indicated times. Cytosolic extracts were examined by Western blotting using the indicated antibodies. *B*, *Iop1*$^{f/f}$; *Rosa26*-creER^{T2} MEFs were treated with 4-hydroxytamoxifen for the indicated times. Cytosolic extracts (20 μg) were incubated with a ^{32}P-labeled RNA probe containing the ferritin heavy chain 5′ IRE and subjected to 5% PAGE (*top panel*). Irp1- and Irp2-induced gel mobility shifts are as indicated. Western blotting of extracts for Irp1 and Irp2 are shown in the *bottom two panels*. *C*, *Iop1*$^{f/f}$; *Rosa26*-creER^{T2} MEFs were treated with 4-hydroxytamoxifen for the indicated times. Whole cell extracts (*top two panels*) or cytosolic extracts (all other panels) were examined by Western blotting using the indicated antibodies. The phosphorylated forms of p38, Jnk1/2, and Erk1/2 are denoted by *p-p38*, *pJnk1/2*, and *pErk1/2*, respectively. Positions of select molecular mass markers (in kDa) are indicated to the *right* of some panels.

same conditions (Fig. 6*B*, *fifth* and *seventh panels* from *top*, respectively). A link between p38 activation and autophagy has been described by others (42). These observations suggest that activation of selective intracellular signaling pathways occurs upon Iop1 loss.

DISCUSSION

A number of studies in recent years have pointed to a role for IOP1 in the mammalian CIA pathway (16, 18). We report here the results of knocking out *Iop1* in the mouse. Based on the results, we make two important conclusions. First, we conclude that Iop1 is a protein essential for life in mammals. This is a significant observation because there exists a homologous protein, Narf/Iop2 (21, 22). Narf shares a number of notable residues with Iop1: first, a set of cysteine residues that, in bacterial hydrogenases, corresponds to an H-cluster that chelates a distinctive active site iron-sulfur cluster; and second, a set of cysteine residues in the N-terminal half of the protein that is present in a ferredoxin-like domain. In contrast to Iop1, which is predominantly cytoplasmic, Narf is a nuclear protein (21). Aside from its capacity to specifically bind to prenylated prelamin A, essentially nothing is known regarding the function of Narf. Importantly, the present studies indicate that the activities of Iop1 and Narf are not redundant and that loss of Iop1 cannot be compensated for by Narf.

The second conclusion from this study is that Iop1 plays an essential role in cytosolic iron-sulfur cluster biogenesis. The inducible genetic ablation approach that is employed in both the *in vivo* studies and the *in vitro* studies examining MEFs support an essential role for Iop1 in this pathway. They differ in approach from previous knockdown studies employing siRNA, which inherently have the possibility of off-target effects. The selectivity of Iop1 for the CIA pathway is reinforced by the absence of effects of *Iop1* deletion on mitochondrial aconitase activity or on that of non iron-sulfur enzymes, such as lactate dehydrogenase or citrate synthase.

The present study contributes to an expanding literature on the role of specific proteins in the mammalian cytosolic iron-sulfur cluster assembly pathway (1, 2). This, in turn, will form the basis for understanding this pathway in the context of human disease. To our knowledge, mutations in the CIA pathway have yet to be linked to human diseases. There is, however, clear evidence already for a link between iron-sulfur cluster biogenesis and human disease (2, 43). Specific human diseases arise from mutations in key proteins involved in iron-sulfur cluster biogenesis, and these diseases target a multitude of organ systems, including hematopoietic, neural, skeletal muscular, and cardiac tissues. The present studies would strongly suggest that complete loss of function mutations in human IOP1 would be incompatible with life. However, the possibility of hypomorphic mutations in IOP1 being linked to human disease remains an intriguing possibility.

Acknowledgments—We thank Dr. Tobias Raabe of the University of Pennsylvania Gene Targeting facility for performing the ES cell electroporation, Dr. Jean Richa of the University of Pennsylvania Transgenic core facility for performing the blastocyst injections, Adrian Flores for assistance in generation of the Iop1 targeting vector, Dr. Neal Copeland (NCI, National Institutes of Health) for recombineering reagents, and Dr. James Alwine (University of Pennsylvania) for the gift of the pSG5-T plasmid.

REFERENCES

1. Lill, R. (2009) *Nature* **460,** 831–838
2. Ye, H., and Rouault, T. A. (2010) *Biochemistry* **49,** 4945–4956
3. Lill, R., and Mühlenhoff, U. (2008) *Annu. Rev. Biochem.* **77,** 669–700
4. Rouault, T. A., and Tong, W. H. (2005) *Nat. Rev. Mol. Cell Biol.* **6,** 345–351
5. Sharma, A. K., Pallesen, L. J., Spang, R. J., and Walden, W. E. (2010) *J. Biol. Chem.* **285,** 26745–26751
6. Roy, A., Solodovnikova, N., Nicholson, T., Antholine, W., and Walden, W. E. (2003) *EMBO J.* **22,** 4826–4835
7. Stehling, O., Netz, D. J., Niggemeyer, B., Rösser, R., Eisenstein, R. S., Puccio, H., Pierik, A. J., and Lill, R. (2008) *Mol. Cell Biol.* **28,** 5517–5528
8. Netz, D. J., Stümpfig, M., Doré, C., Mühlenhoff, U., Pierik, A. J., and Lill, R. (2010) *Nat. Chem. Biol.* **6,** 758–765
9. Netz, D. J., Pierik, A. J., Stümpfig, M., Mühlenhoff, U., and Lill, R. (2007) *Nat. Chem. Biol.* **3,** 278–286
10. Zhang, Y., Lyver, E. R., Nakamaru-Ogiso, E., Yoon, H., Amutha, B., Lee, D. W., Bi, E., Ohnishi, T., Daldal, F., Pain, D., and Dancis, A. (2008) *Mol. Cell Biol.* **28,** 5569–5582
11. Balk, J., Aguilar Netz, D. J., Tepper, K., Pierik, A. J., and Lill, R. (2005) *Mol.*

Cell Biol. **25,** 10833–10841
12. Balk, J., Pierik, A. J., Netz, D. J., Mühlenhoff, U., and Lill, R. (2004) *EMBO J.* **23,** 2105–2115
13. Tong, W. H., and Rouault, T. (2000) *EMBO J.* **19,** 5692–5700
14. Tong, W. H., and Rouault, T. A. (2006) *Cell Metab.* **3,** 199–210
15. Tong, W. H., Jameson, G. N., Huynh, B. H., and Rouault, T. A. (2003) *Proc. Natl. Acad. Sci. U.S.A.* **100,** 9762–9767
16. Song, D., Tu, Z., and Lee, F. S. (2009) *J. Biol. Chem.* **284,** 35297–35307
17. Land, T., and Rouault, T. A. (1998) *Mol. Cell* **2,** 807–815
18. Song, D., and Lee, F. S. (2008) *J. Biol. Chem.* **283,** 9231–9238
19. Hausmann, A., Aguilar Netz, D. J., Balk, J., Pierik, A. J., Mühlenhoff, U., and Lill, R. (2005) *Proc. Natl. Acad. Sci. U.S.A.* **102,** 3266–3271
20. Srinivasan, V., Netz, D. J., Webert, H., Mascarenhas, J., Pierik, A. J., Michel, H., and Lill, R. (2007) *Structure* **15,** 1246–1257
21. Barton, R. M., and Worman, H. J. (1999) *J. Biol. Chem.* **274,** 30008–30018
22. Huang, J., Song, D., Flores, A., Zhao, Q., Mooney, S. M., Shaw, L. M., and Lee, F. S. (2007) *Biochem. J.* **401,** 341–352
23. Copeland, N. G., Jenkins, N. A., and Court, D. L. (2001) *Nat. Rev. Genet.* **2,** 769–779
24. Liu, P., Jenkins, N. A., and Copeland, N. G. (2003) *Genome Res.* **13,** 476–484
25. Yagi, T., Ikawa, Y., Yoshida, K., Shigetani, Y., Takeda, N., Mabuchi, I., Yamamoto, T., and Aizawa, S. (1990) *Proc. Natl. Acad. Sci. U.S.A.* **87,** 9918–9922
26. Laird, P. W., Zijderveld, A., Linders, K., Rudnicki, M. A., Jaenisch, R., and Berns, A. (1991) *Nucleic Acids Res.* **19,** 4293
27. Xu, J. (2005) in *Current Protocols in Molecular Biology* (Ausubel, F. M., ed) pp. 28.1.1–28.1.8, John Wiley & Sons, Inc., New York
28. Yu, Y., and Alwine, J. C. (2002) *J. Virol.* **76,** 3731–3738
29. Li, X., Sutherland, S., Takeda, K., Fong, G. H., and Lee, F. S. (2010) *Blood Cells Mol. Dis.* **45,** 9–19
30. Seibler, J., Zevnik, B., Küter-Luks, B., Andreas, S., Kern, H., Hennek, T., Rode, A., Heimann, C., Faust, N., Kauselmann, G., Schoor, M., Jaenisch, R., Rajewsky, K., Kühn, R., and Schwenk, F. (2003) *Nucleic Acids Res.* **31,** e12
31. Rouault, T. A. (2006) *Nat. Chem. Biol.* **2,** 406–414
32. Muckenthaler, M. U., Galy, B., and Hentze, M. W. (2008) *Annu. Rev. Nutr.* **28,** 197–213
33. Clarke, S. L., Vasanthakumar, A., Anderson, S. A., Pondarré, C., Koh, C. M., Deck, K. M., Pitula, J. S., Epstein, C. J., Fleming, M. D., and Eisenstein, R. S. (2006) *EMBO J.* **25,** 544–553
34. Wang, J., Fillebeen, C., Chen, G., Biederbick, A., Lill, R., and Pantopoulos, K. (2007) *Mol. Cell Biol.* **27,** 2423–2430
35. Meyron-Holtz, E. G., Ghosh, M. C., and Rouault, T. A. (2004) *Science* **306,** 2087–2090
36. Thomson, A. M., Rogers, J. T., and Leedman, P. J. (2000) *J. Biol. Chem.* **275,** 31609–31615
37. Henderson, B. R., and Kühn, L. C. (1995) *J. Biol. Chem.* **270,** 20509–20515
38. Riedl, S. J., and Shi, Y. (2004) *Nat. Rev. Mol. Cell Biol.* **5,** 897–907
39. He, C., and Klionsky, D. J. (2009) *Annu. Rev. Genet.* **43,** 67–93
40. Ravikumar, B., Futter, M., Jahreiss, L., Korolchuk, V. I., Lichtenberg, M., Luo, S., Massey, D. C., Menzies, F. M., Narayanan, U., Renna, M., Jimenez-Sanchez, M., Sarkar, S., Underwood, B., Winslow, A., and Rubinsztein, D. C. (2009) *J. Cell Sci.* **122,** 1707–1711
41. Raman, M., Chen, W., and Cobb, M. H. (2007) *Oncogene* **26,** 3100–3112
42. McClung, J. M., Judge, A. R., Powers, S. K., and Yan, Z. (2010) *Am. J. Physiol. Cell Physiol.* **298,** C542–549
43. Sheftel, A., Stehling, O., and Lill, R. (2010) *Trends Endocrinol. Metab.* **21,** 302–314